Rheological Investigations on Frequency Selective Surface Carbon Composite Microwave Absorber

Priyanka[1], Prashant S. Alegaonkar[1,*] Himangshu B. Baskey[2,*]

[1] *Department of Physics, School of Basic Sciences, Central University of Punjab, Bathinda, Punjab 151401, India*
[2]*Stealth & Camouflage Division, Defence Material Store R & D Establishment, DRDO, Kanpur, UP 208013, India*

Supplementary file

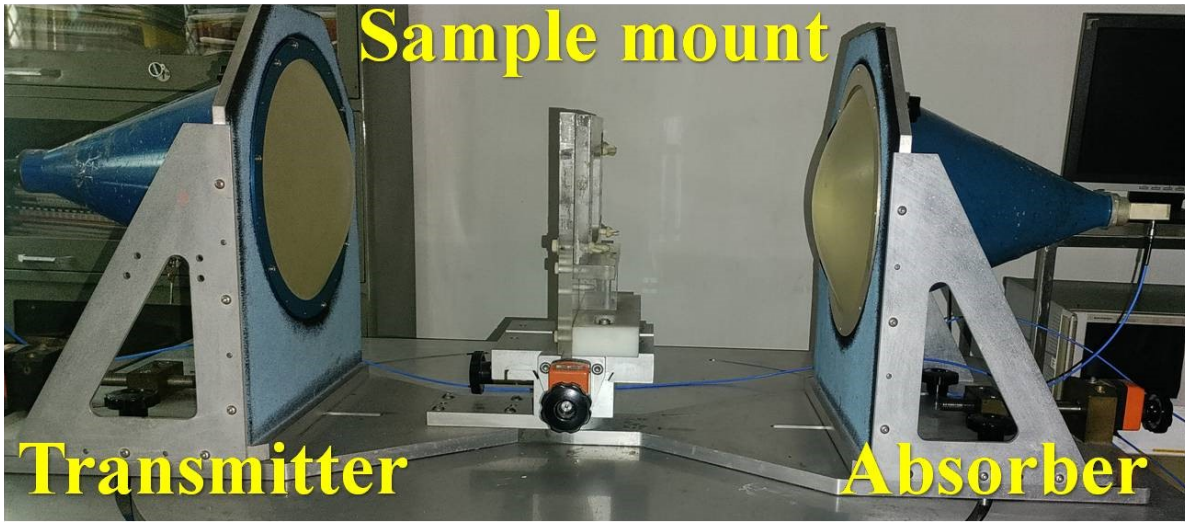

Figure S1: Experimental setup of Vector network analyzer (VNA) equipped with horn shape transmitter, receiver I/O ports, and sample mount assembly.

Figure S1 shows the spot focusing horn lens antenna consists of two equal plano-convex dielectric lenses mounted back-to back in order to focus the incident electromagnetic power at a focal length of 30.5 cm. The laminates were placed on sample holder which was positioned at the common focal plane of the antennae, Through-Reflect-Line (TRL) calibration has been carried out before performing the constitutive measurements in order to avoid systematic errors. Finally, transmission and reflection measurements were performed to obtain dielectric properties of test specimens.

Table S1: Elemental composition of raw starting material and ink composite

S.N.	wt %	CB	Ag	O
1.	CB	99.3%	-	-
2.	Ag NPs	-	81.5%	3.4%
3.	Ink Composite	51.15%	48.85%	-

*Corresponding author: Prashant S. Alegaonkar (Email: prashant.alegaonkar@cup.edu.in)

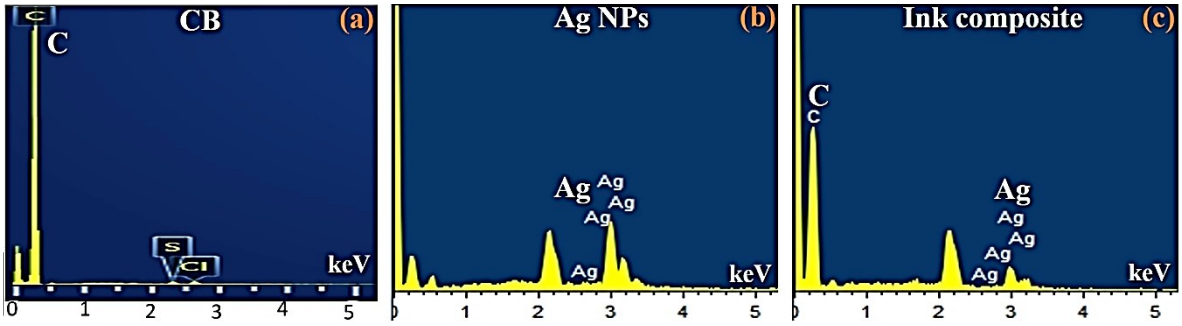

Figure S2: EDAX spectra displaying elemental composition of (a) raw CB, (b) Ag NPs, and (c) ink composite.

For analysing elemental composition and comparing them with pristine counter parts EDAX /SCM measurements were performed afresh. Figure S2 shows recorded EDAX profiles for all the three specimens. Corresponding EDAX composition is displayed in Table S1. Analysis revealed that, ration and proportion of elements played important role in tunning the surface resistivity of the ink composite. Notably, the optimized composition has been displayed for reference.

Figure S3 (a) shows reflection loss performance with respect to varying sheet resistivity [235-275 Ω/sq.], it can be observed from the corresponding figure that as the sheet resistance value is increased absorptivity increases, reflection minima of 33.5dB is attained corresponding to 275 Ω/□, further resonant frequency shifts gradually towards the left end of frequency band. The thickness of various laminates have been represented by t_1, t_3 and t_v, sample thickness t_1 and t_3 refer to the thickness of lossy dielctric laminates, t_2, t_v refers to sample thickness of GFRP and Roha cell foam respectively, whereas t_s represent thickness of FSS layer. It can be observed from Figure S3(b) that increase in foam thickness (tv) improve the absorption performances and absorption maxima shifts towards the lower end of frequencies. Figure S3 (c) shows reflection loss performance with varying laminates thickness t3, it can be observed that increasing sample thickness, absorption value decreases and reflection minima shifts towards lower end of frequency. Similar reflectivity performance is observed by varying laminate thickness (t_3) as shown in Figure S3(d), after various optimization, thickness of 2.8mm, 0.2mm, 0.2 mm have been chosen for t_v, t_3, t_1 respectively. Figure S3(e) shows variation in reflection loss performances of absorber with varying unit cell dimension length (L), it can be observed for 10.4mm, maximum absorptivity is attained. Figure S3(f) shows absorber performances by varying carbon black contents (5-15%) of lossy laminates, it can be observed that corresponding to 5% CB laminate, maximum absorption of 25.03dB is observed corresponding to 10 GHz, further increase in the filler concentration shifts reflection minima towards lower end of frequency region.

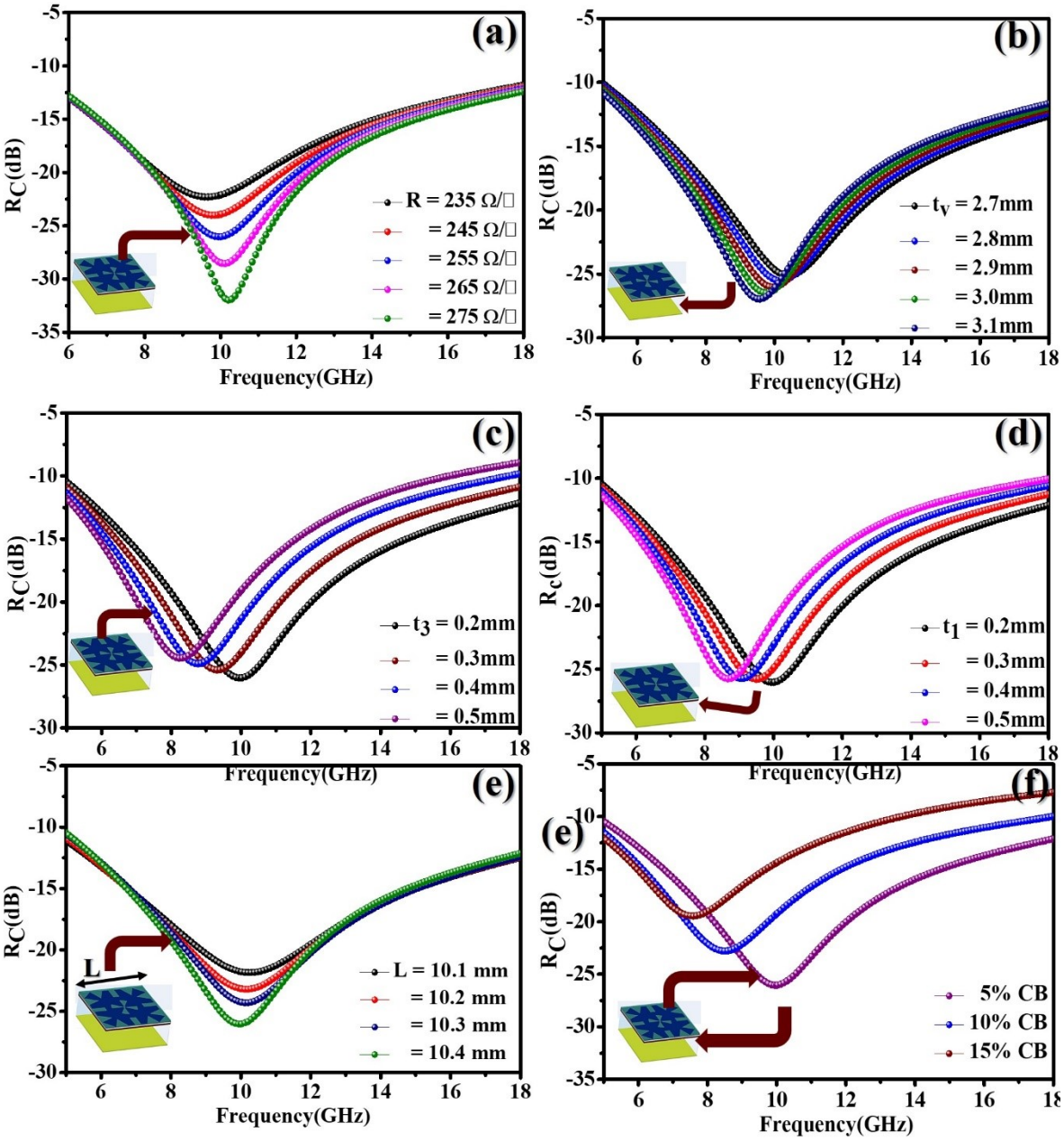

Figure S3: R_C performance of the absorber for (a) variable sheet resistance of FSS pattern, (b) thickness of Roha spacer (tv), (c) thickness of composite laminates (t_3), (d) (t_1), (e) unit cell size (L) in mm, and (f) wt.% composition of carbon black in composite laminates.

Figure 6 (a) and (b) shows the induced surface current density response of the cell to the incident TE mode and discussed in detail in the main text. Figure S4 shows distribution of surface current induced at front and rear surface of the absorber. In image (a), the front portion of the cell shows larger voids on the unit cell indicating no or feeble current density. This shows that TM mode is weakly coupled due to non-uniform current density distribution. However, at the centre and on the edges of the cell the current density reaches a moderate value between 8-10 A/m. The direction of the current is vectorially opposite to the incident TM vector. At rear surface, the surface current density was found to be uniform achieving a value between 7-8

A/m. in this case also the direction vectors are opposite. This shows that coupling of TM mode of the cell is weak as compare to TE mode.

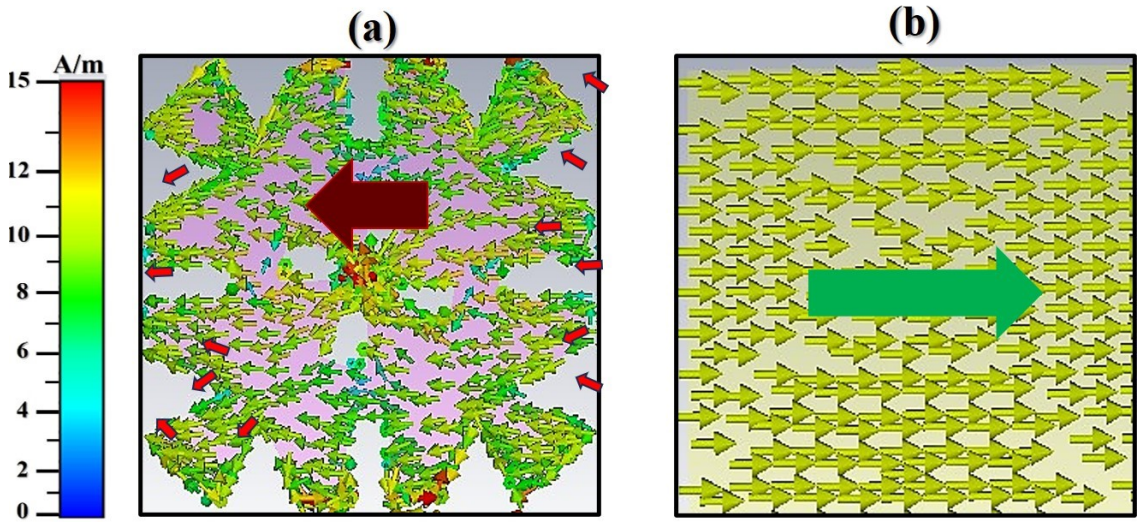

Figure S4: Surface current distribution (a) front and (b) rear surface of the hybrid absorber for TM mode (data @ 10 GHz).

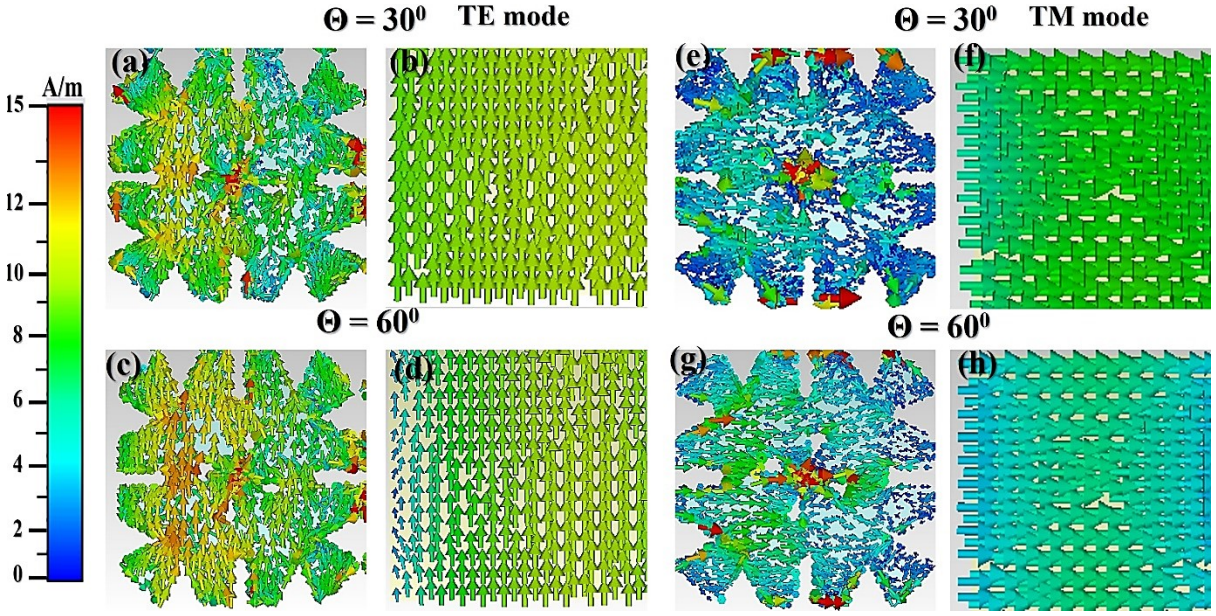

Figure S5: Surface current distribution (a), (c) and (e), (g) @ front and (b), (d) and (f), (h) @ rear side of the hybrid absorber. Corresponding mode and angle of incidence has been displayed. (data @ 10 GHz).

Figures S5 (a) and (b) display the front and rear surface current density distribution at an angle @ various angles of incidence (30^0 and 60^0) for both TE and TM modes. At the front surface, the charge puddling is seen to be completely inhomogeneous with a non-symmetric charge distribution across the cell. No distinct gradient pattern is recorded at the rear surface for these angles in both modes. This appears to contribute to the reduction in the Rc losses with

the appearance of the lossy shoulder at high frequency. Particularly, at an angle of 60^0, as depicted in Figure S5 (c) and (d), the current distribution on the front surface remains unchanged in comparison to 0^0. The direction of surface current on the front surface is completely opposite compared to 0^0, and the direction for both the front and rear surfaces appears to be the same. This suggests that there is no current cancellation effect. Therefore, an increase in the angle of incidence will lead to a reduction in Rc losses due to the weakening of the current cancellation effect. The behaviour of TM is observed to be consistent with TE (Figure S5 (e)-(h)).

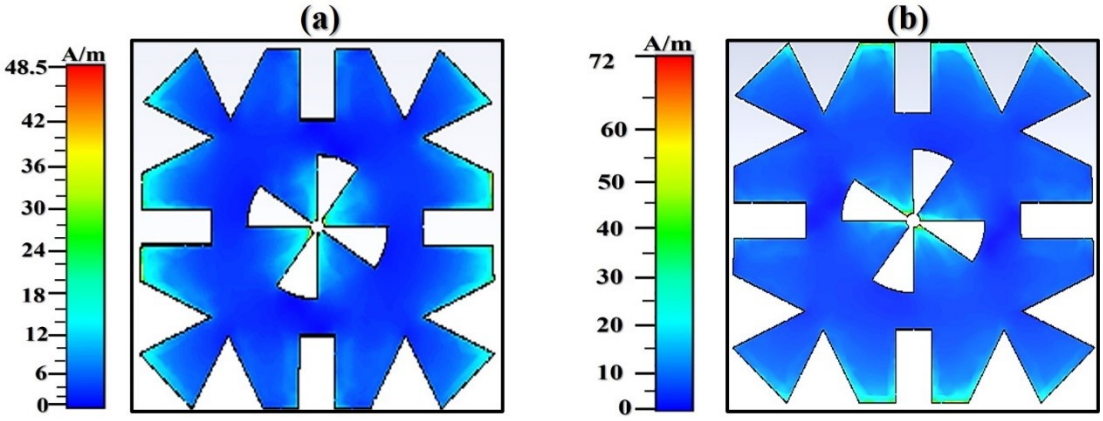

Figure S6: Magnetic field distribution for (a) TE, (b) TM mode.

Figure S6(a) and (b) displays the magnetic field distributions for TE and TM modes respectively at the resonant frequency of 10 GHz, it has been observed that for the TE mode, the magnetic field is concentrated on the left and right sides of the resistive FSS pattern, while for the TM mode, maximum magnetic field is concentrated at the upper and lower edges of FSS geometry showing intensity ranging from 0-72 A/m.

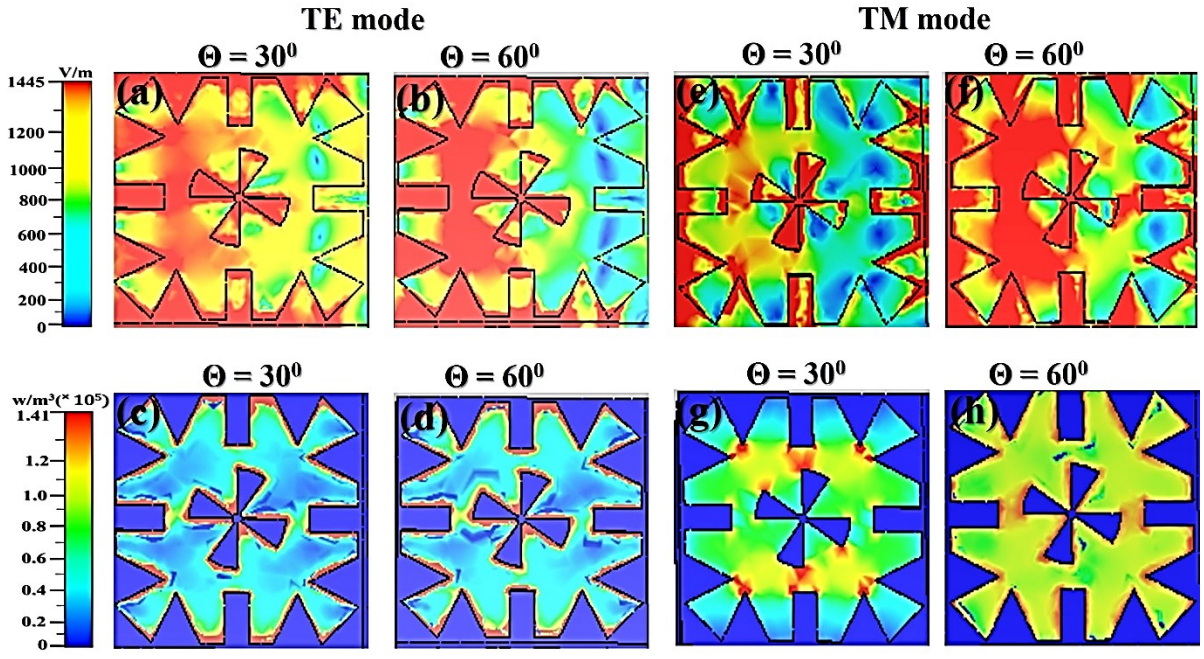

Figure S7: (a)-(b) electric field distribution,(c)-(d) power loss at front surface for $\Theta = 30^0$ and 60^0 (TE mode) correspondingly field distribution and power loss topology simulted in (e)-(h). Scale bar for each parametric profile is shown on the left-hand side of each pan.

Figure 57 (a)-(b) shows distribution of electric field in responce to incident TE mode at $\Theta = 30^0$ and 60^0. Analysis revelted that electric field distribution is a symmetric over the cell. With increase in angle of incidance, the induced electric field is found to be intensified aymmetrically across the cell. Similar trend has been observed for incident TM mode (Figure S7 (e)-(f)). For power distribution, showen in Figure S7 (c)-(d), the increase in angle of incedance has not brought much change in power loss for TE mode. Mostly for this mode, the losses have been observed on the edges of the blade or on the periferial fetures of the cell. This shows that, electric field is tightly coupled with the cell. However, for the TM mode, different scenario has been seen with increase in angle (Figure S7 (g)-(h)). The power was found to be distributed in the neighbourhood of fan blades. For lower angle ($\Theta = 30^0$) the hotspot have been seen away from the fan blades. For higher angle, the intensity of these hotspot is found to be diminished with emergance of low power patches at several places of the cell pattern.

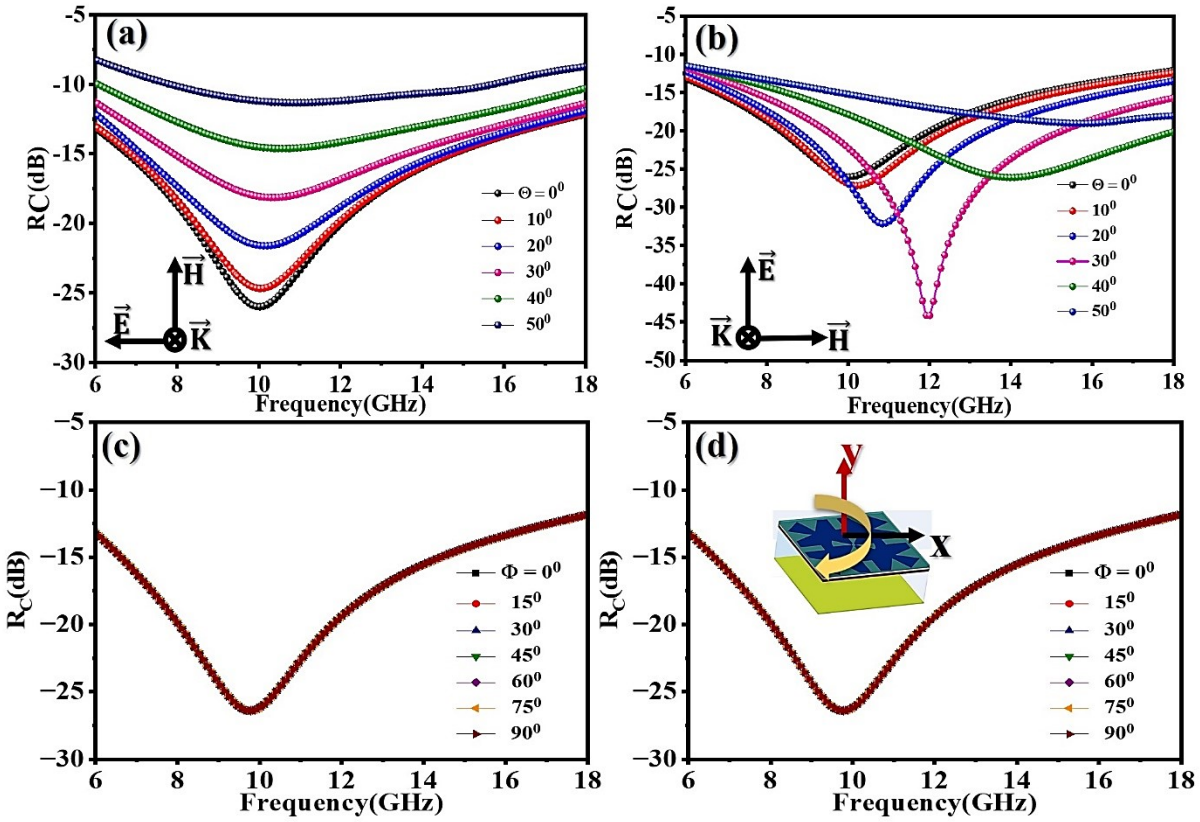

Figure S8: R_c performance for (a) TE and (b) TM modes at variable angles of incidence $\Theta = 0 - 50^0$, angular rotation $\Phi = 0 – 90^0$ for (c) TE and (d) TM modes.

The absorber has been illuminated by mode TE and TM at an incident wave vector, $\vec{K}$, with variable angles of incidence ranging from 0° to 50°. Figure S8 (a) and (b) show patterns of R_c losses over 6-18 GHz. Inset shows plane of the oscillatory electric and magnetic vector components of the field with reference to the incident, $\vec{K}$, propagation vector. With subsequent

increases in the value of Θ, the dB levels were, correspondingly, found to be decreased monotonically. At Θ= 50^{o}, the designed absorber has attained a loss value of - 10 dB. Physically, the absorption of a mode is associated with the generation of the displacement currents in the absorber. The main resonance peak, which appeared at ~ 10 GHz, indicates that there is a coupling of the incident TE mode with the displacement currents generated within the absorber. The overall response of the absorber for TM mode is significantly different than TE. A 10-20^{o} offset in losses with respect to Θ values has been observed for TM, as seen in Figure S8(b). At Θ = 0^{o}, losses were reported to be - 26.5 dB (TM/TE). Thereafter, an increase up to - 45 dB has been seen at Θ = 20^{o} to 30^{o}, followed by a gradual decay to a – 10 dB level at Θ = 50^{o}. Notably, except at Θ = 0^{o}, where losses were comparable with TE, mode. TM dB levels remained higher than TE for other angles of incidences. This indicates that the coupling of TM with the absorber is stronger than TE over the simulated 6-18 GHz. Unlike TE, no splitting in the resonance peak is seen. This indicates a strong, singular displacement current source in the absorber cell. Figure S8(c) and (d), respectively, show TE and TM loss spectrum over a 6 – 18 GHz for Φ = 0 – 90^{0}. Insect in (d) shows the rotation of the absorber cell schematically. The loss spectrum of both the modes are found to be identically symmetric with highest losses reported near resonance. For larger frequency regions the losses have reached to a value ~ -10dB.